Characterization of the adsorption of H_2 and N_2 on activated carbon used as an adsorbent in cryosorption pumps

Nick P. Zobel,[1,a] Stefan Wilfert,[1] Klaus Blaum,[2] Sven M. Elbert,[3] Michael Mastalerz,[3]
and Peter J. Spiller[1]

AFFILIATIONS

[1]GSI Helmholtzzentrum für Schwerionenforschung, Planckstrasse 1, Darmstadt D-64291, Germany
[2]Max-Planck-Institut für Kernphysik, Saupfercheckweg 1, Heidelberg D-69117, Germany
[3]Institute of Organic Chemistry, Heidelberg University, Neuenheimer Feld 272, Heidelberg D-69120, Germany

[a]Author to whom correspondence should be addressed: n.zobel@gsi.de

ABSTRACT

The adsorption behavior of H_2 and N_2 on two types of granular activated carbon, SC2 and Aquacarb 208C, was investigated in the cryogenic temperature range using automated high-vacuum gas adsorption measurements. The aim of the study was to identify a suitable material for potential use as an adsorbent in cryosorption pumps, as required for the SIS100 accelerator at the Facility for Antiproton and Ion Research in Darmstadt, Germany. To characterize the adsorption process, isotherms were measured and evaluated using several well-established theoretical adsorption models. These models enabled the determination of specific fundamental surface characteristics of the activated carbons, such as pore volume, pore surface, and adsorption energies. Among the models tested, the Dubinin–Radushkevich (DR-)theory best described the adsorption behavior of hydrogen on both adsorbents at subcritical temperatures and low pressures while enabling predictions under conditions relevant to cryosorption pumps. The DR analysis yielded temperature-independent pore volumes of 388 cm³/g (STP) for SC2 and 417 cm³/g (STP) for 208C. Based on this finding, the SIS100 cryosorption pumps were equipped with 208C as the adsorbent, with one pump exhibiting a maximum hydrogen uptake capacity of approximately 205 mbar l at 4.5 K.

I. INTRODUCTION

The SIS100 heavy ion synchrotron, the main accelerator of the FAIR (Facility for Antiproton and Ion Research) complex at the GSI Helmholtz Center for Heavy Ion Research in Darmstadt, Germany, uses almost exclusively superconducting magnets for beam guidance.[1,2] As a result, 4/5 of the entire beamline vacuum system is maintained under cryogenic conditions at temperatures between 4.5 and 20 K.[1,3] Cooling to such low temperatures typically allows the generation and long-term stable maintenance of extremely low pressures less than 1×10^{-12} mbar in these systems by cryopumping.[4] With the exception of hydrogen and helium, all other vacuum-relevant gas species can be cryocondensed to their saturated phase on the surface of the chamber walls with virtually unlimited pumping capacity, since their saturation vapor pressures

are well below 1×10^{-12} mbar at these temperatures.[4] However, hydrogen, which is typically the predominant gas species in UHV/XHV systems, and helium, which may leak as a refrigerant in low-temperature vacuum systems, cannot be cryocondensed to their saturated phase. This limitation is due to their relatively high saturation vapor pressures, even at temperatures as low as 4.2 K.[5] Gas load-independent hydrogen pumping into the saturated phase, where saturation vapor pressures drop to around 1×10^{-12} mbar, would require temperatures of about 2 K, while for helium, a few hundred millikelvin would be necessary. In cryogenic accelerator systems using normal-fluid helium at 4.2 K, both gas species can only be pumped by cryosorption in the submonolayer region, i.e., the process preceding cryocondensation, where the vapor pressure established still depends on the gas coverage of the cryogenic

pumping surface. In order to prevent the vapor pressure from reaching saturation, it is essential to keep the surface coverage significantly below one monolayer.[4,5]

To ensure this, there are practically only two possible approaches. The cold vacuum system is either designed to protect against excessive H_2 or He gas loads, or the cryogenic pumping surface area for gas particle adsorption is maximized. The latter method is used by cryosorption pumps, which typically use granular adsorbents with large specific surfaces.[3] At sufficiently low temperatures, these granular adsorbents are capable of adsorbing large quantities of gas, making them perfect gas sinks. Cryogenic accelerator vacuum systems operating at LHe or higher temperatures, such as those of the SIS100, where ultrahigh or extremely high vacuum pressures are required for beam operation, typically need auxiliary cryosorption pumps to provide additional pumping speed for hydrogen and helium.[3,4] Cryosorption pumps with highly porous adsorbents have been proven to be particularly effective. Extensive R&D studies in the context of nuclear fusion applications have shown that activated carbon, especially coconut-based types, offers the most favorable cryosorption performance for H_2 and He.[6–9] For the SIS100 cryosorption pumps, two specific types of activated carbon were therefore identified as suitable candidates.

As the residual gas atmosphere in LHe-cooled vacuum systems consists primarily of hydrogen, this study focused on characterizing the hydrogen adsorption behavior of both adsorbents, with emphasis on their adsorption capacities, pore sizes, and pore distributions. Adsorption measurements with helium were not conducted, as the experimental setup lacked the capability to cool the adsorbent samples to temperatures below 15 K—the range most relevant for this gas.

The combination of extreme environmental conditions and the generation of ultrahigh or even extremely high vacuum pressures render the direct study of gas adsorption on activated carbon-based adsorbents in cryogenic systems nearly impossible, or at least a considerable technical and instrumental challenge. In order to nonetheless characterize the pumping properties of the adsorbents under typical operating conditions of the accelerator, measurements were performed in a vacuum pressure range accessible to current techniques. The results were then analyzed using widely accepted adsorption theories. By linking the observed adsorption behavior to a known model, the adsorption at ultralow and extremely low pressures—otherwise inaccessible to direct measurements—can be theoretically predicted. The adsorption behavior of N_2 on both adsorbents was studied at LN_2 temperatures, as this is relevant for the consideration of the gas preloading of the pumps during the cool-down process.

II. THEORETICAL MODELS FOR GAS ADSORPTION ON POROUS SOLIDS

Adsorption isotherms are essential for characterizing gas adsorption on porous materials, as they describe the relationship between the adsorbed amount and the gas pressure. For clarity in the interpretation of our measurements, the models applied in this study are briefly summarized below. The isotherm model equations used here apply exclusively to the case of nondissociative adsorption. Detailed treatments are available in the cited literature.

A. Langmuir theory

The Langmuir model[10] is based on two key assumptions: (1) adsorption occurs as a single monolayer and (2) the adsorption energy is uniform across all surface sites and independent of surface coverage. This leads to the Langmuir isotherm,

$$\frac{V_{\text{ads}}}{V_{\text{mono}}} = \frac{bp}{1+bp}, \tag{1}$$

where V_{ads} is the adsorbed volume, V_{mono} is the volume of the adsorbate in the monolayer, p is the pressure, and $b(T)$ is the temperature-dependent adsorption coefficient. In practice, the linearized form of Eq. (1),

$$\frac{p}{V_{\text{ads}}} = \frac{1}{bV_{\text{mono}}} + \frac{1}{V_{\text{mono}}}p, \tag{2}$$

is preferred, as plotting (p/V_{ads}) vs p yields a straight line, from which the slope provides $1/V_{\text{mono}}$, allowing V_{mono} to be determined directly. Once V_{mono} is determined, the monolayer surface area A_{mono} can be calculated via

$$A_{\text{mono}} = s\rho_{\text{mol}}V_{\text{mono}}N_A, \tag{3}$$

with N_A being Avogadro's number, ρ_{mol} being the molar density, and s being the cross-sectional area of the gas particles.

B. BET theory

To account for multilayer adsorption, Brunauer, Emmett, and Teller extended the Langmuir model to encompass multi-layer adsorption.[10] The central result of this extension is the so-called BET isotherm,

$$\frac{V_{\text{ads}}}{V_{\text{mono}}} = \frac{C\frac{p}{p_s}}{\left(1-\frac{p}{p_s}\right)\left(1-\frac{p}{p_s}+C\frac{p}{p_s}\right)}, \tag{4}$$

in which C is the temperature-dependent BET constant and p_s represents the saturation vapor pressure of the adsorbate at temperature T. For practical applications, the linearized BET form is used,

$$\frac{p/p_s}{V_{\text{ads}}(p_s - p)} = \frac{1}{V_{\text{mono}}C} + \frac{C-1}{V_{\text{mono}}C}\frac{p}{p_s}, \tag{5}$$

for which a linear fit, as in the Langmuir theory, can be performed.

C. Dubinin-radushkevich (DR-)theory

The Dubinin–Radushkevich (DR) theory[11] assumes that adsorption occurs via micropore filling rather than layer-by-layer accumulation. Micropore sizes are assumed to follow a Gaussian distribution, with a pressure-dependent adsorption potential ϕ within the pores. Mathematically, the theory is described by

$$\frac{V_{\text{ads}}}{V_p} = \exp\left[-D\phi^2\right] = \exp\left[-D\left(k_bT\ln\frac{p}{p_s}\right)^2\right], \tag{6}$$

with k_b being the Boltzmann constant, T the temperature, $D = 1/E_0^2$ the DR constant, and E_0 the characteristic adsorption energy. In the DR equation, the monolayer volume, V_{mono}, is replaced by the micropore volume, V_p, which is not the same. The characteristic adsorption energy E_0 is treated as independent of V_{ads}, since D is assumed to be a constant. Experimental data are often analyzed using the linearized isotherm equation,[5,12] i.e.,

$$\ln V_{ads} = -D\left[k_b \ln \frac{p}{p_s}\right]^2 + \ln V_p.$$

According to an empirical correlation found by Dubinin and Stoeckli,[13] the average micropore half-width $\frac{d}{2}$ of porous, carbon-based adsorbents can be deduced if the characteristic energy E_0 is known. It reads

$$\frac{d}{2} = \frac{0.135\,\text{eV} \quad \text{nm}}{E_0}. \qquad (7)$$

D. t-plot method

The t-plot method[14] is a widely used analytical tool in adsorption studies. By employing this technique, key parameters describing the adsorption behavior of gases on adsorbent materials can be estimated by comparing the experimental data to a reference isotherm—an empirical curve relating the film thickness t of a nitrogen layer adsorbed on a smooth, nonporous surface at 77 K to the pressure ratio p/p_s. Through this comparison, the micropore volume as well as the external surface area, which corresponds to the area accessible to multilayer adsorption outside of micropores, can be determined. However, because the t-plot method depends on a gas-specific thickness curve, it is most commonly applied to nitrogen adsorption at 77 K, where a well-established reference curve is available.

E. Density functional theory (DFT)

Density Functional Theory (DFT)[15] is a statistical-mechanical approach to determining the pore size distribution in materials. DFT determines the equilibrium density profile of the adsorbed phase by minimizing the system's free energy, accounting for wall-fluid interactions. This method is used with computer support. The algorithm uses precomputed kernels to model isotherms for pores of various sizes. Experimental adsorption data are then deconvoluted against these isotherms to obtain high-resolution pore size distributions. In this analysis, quenched solid DFT (QSDFT)[16] kernels—an extension of classical DFT that accounts for surface roughness and pore geometry—were applied to 77 K nitrogen isotherms to determine pore size distributions.

III. EXPERIMENTAL SETUP

A. Activated carbon samples and gases used

Two activated carbon samples, SC2 and Aquacarb 208C, produced by Chemviron©, were used in this study.

Both carbons were derived from coconut shells and activated using a high-temperature steam process. Properties for SC2 were characterized at the Karlsruhe Research Center,[17] data for 208C

TABLE I. Properties of activated carbons of the SC2 and 208C types (Refs. 17 and 18).

Property	SC2	208C	Unit
Spec. heat (100 °C)	0.80–1.00	N/A	kJ/(K kg)
Bulk Density	0.45–0.48	0.48	g/cm^3
Apparent density	0.80–0.85	0.88	g/cm^3
Skeleton density	2.0–2.2	2.15	g/cm^3
Hardness	95–99	98	%
Size (<0.6 mm)	5	5	%
Size (>1.7 mm)	10	8	%
Size (in between)	85	87	%

was provided directly by the manufacturer.[18] Table I lists key physical properties of the two carbon grades. Scanning electron microscope images are exemplarily shown in Fig. 1(a) for SC2 and Fig. 1(b) for 208C.

Hydrogen and nitrogen gases (99.999% purity) were used. Thermophysical properties, such as critical temperature and pressure, were obtained from the CoolProp database.[19]

B. High-vacuum adsorption analyzer autosorb iQ3

Adsorption measurements were conducted using the Autosorb iQ3 (Quantachrome©), an automated gas sorption system equipped with integrated gas and vacuum control, a rotary vane backing pump, and a turbomolecular pump, as can be seen in Fig. 2. Measurements between 16 and 300 K were enabled by a cryostat with temperature control.

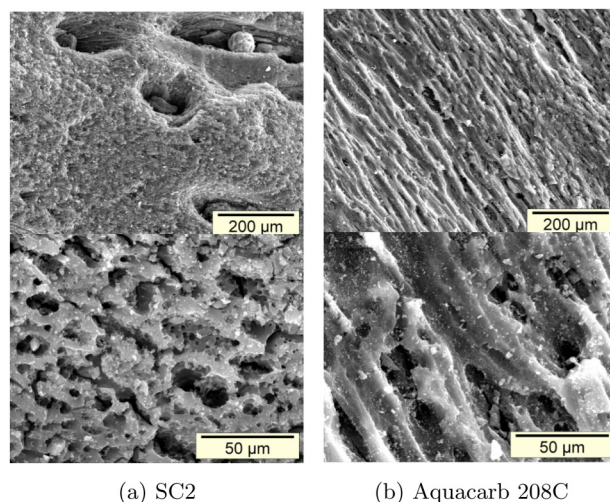The full measurement procedure, including calibration and cryogenic adjustments, is detailed by Zobel.[20]

(a) SC2   (b) Aquacarb 208C

FIG. 1. Scanning electron microscope images of activated carbon samples: (a) SC2 and (b) Aquacarb 208C.

FIG. 3. 77 K nitrogen isotherms for activated carbon SC2 and 208C.
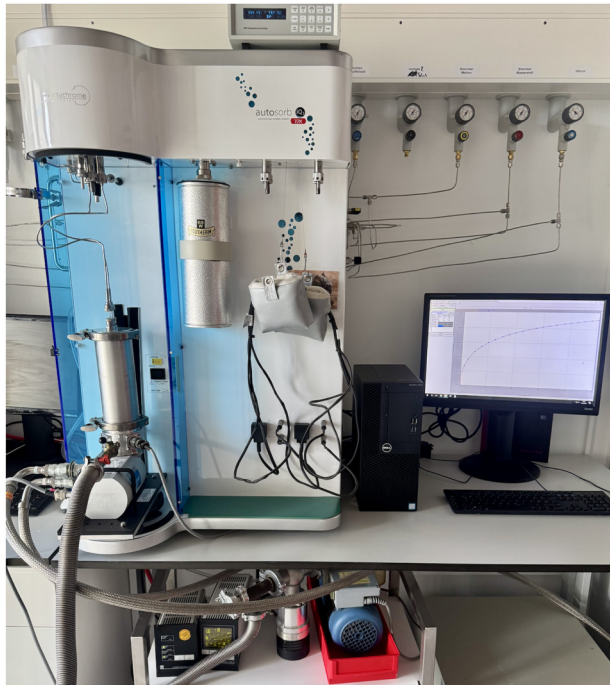

FIG. 2. Autosorb iQ3 configured to measure isotherms at cryogenic temperatures.

IV. EXPERIMENTS AND MEASURING RESULTS

The results of N_2 and H_2 adsorption measurements presented below were obtained using the same measuring cells and the same activated carbon samples.

A. Adsorption capacity measurements with nitrogen

First, nitrogen isotherms were measured for both samples at the boiling point of nitrogen. These 77 K N_2 isotherms are standard measurements, typically obtained by cooling with liquid nitrogen and leveraging its low cost and ease of handling. The results of these measurements are given in Fig. 3 as $\log p$ vs $\log V_{ads}$ plots. Both isotherms show a strongly nonlinear relationship in the double-logarithmic representation. Pore condensation near 1000 mbar is evident, caused by capillary condensation close to the boiling point, which artificially increases the measured adsorption. This results from the software assuming gas-phase density, while nitrogen begins to liquefy, leading to a sharp increase in actual density.

In this preliminary phase, the samples were characterized using multiple analytical methods based on the 77 K nitrogen isotherm. Together with the results from Sec. V, this provides a quantitative benchmark for other cryopumping materials.

The following evaluations were carried out using the ASIQWIN Software of the Autosorb iQ3, which performs the fitting of the graphs, calculates the parameters, and executes a DFT calculation. All calculations are based on the linearized isotherms from Sec. II
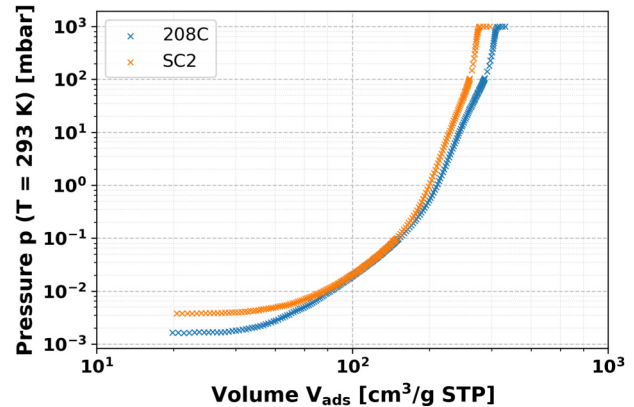
and are detailed in the software manual.[21] The adsorbed volume (per gram of adsorbent) at STP V_{ads} was converted into the adsorbed gas mass (per gram of adsorbent) W using the molar mass M_{mol},

$$W = V_{ads} M_{mol} \cdot \frac{1\,\text{mol}}{22\,400\,\text{cm}^3}. \tag{8}$$

For instance, in the case of the BET theory, the value $(W(p_{rel} - 1))^{-1}$ was plotted against the relative pressure, and the linear correlation in the relative pressure range between 0.05 and 0.3 was sought.[17]

The monolayer volumes are then determined using a linear fit of the points (cf. Fig. 4) according to Eq. (5) and the monolayer areas according to Eq. (3).
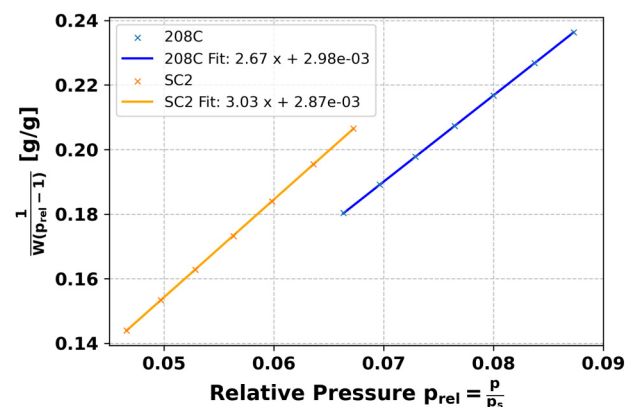

FIG. 4. Adsorption isotherms for activated carbon SC2 and 208C evaluated according to the linearized BET equation: Shown is $\frac{1}{W(p_{rel}-1)}$ against p_{rel} for the measurement data selected with the BET wizard and the best-fit line according to Eq. (5).

TABLE II. Surface characterization parameters for activated carbon SC2 and 208C, determined from the 77 K nitrogen isotherm using various analytical methods. For all fits: Error < 0.5% and R^2 > 0.98.

Method	SC2 Pore vol. (cm³/g)	SC2 Pore surf. (m²/g)	208C Pore vol. (cm³/g)	208C Pore surf. (m²/g)
Langmuir-plot[a]	0.481	1352	0.566	1594
BET-plot[a]	0.408	1149	0.462	1301
DR-plot[b]	0.422	1188	0.470	1322
t-plot[b]	0.464	1137[c]	0.542	1284[c]
DFT analysis	0.422	1120	0.522	1246

[a]According to the theory, the determined parameters are the monolayer volume V_{mono} and the monolayer surface area A_{mono}.

[b]According to the theory, the determined parameters are the microporous volume V_p and the microporous surface area A_p.

[c]Difference between the external surface area from Table III and BET surface area.
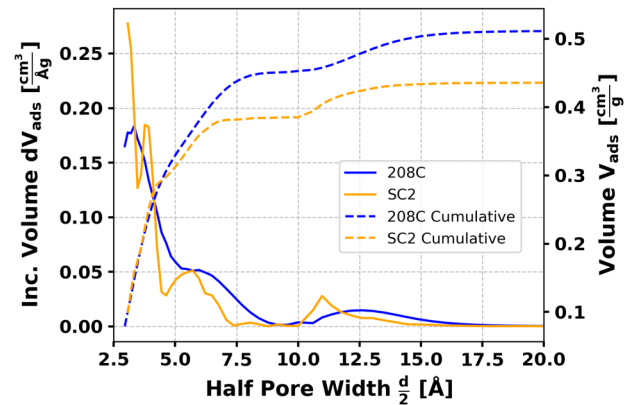

FIG. 5. Pore size distribution for activated carbon SC2 and 208C obtained by DFT analysis. Solid lines represent the incremental pore volume distribution $\frac{dV}{d(d/2)}$ and dashed lines show the cumulative pore volume as a function of half pore width.

The results of the various adsorption theories and the correlation coefficients of the fits are presented in Tables II and III.

Finally, the pore size distribution of both samples was determined using QSDFT calculations with consideration of slit, cylindrical, and spherical pores.

The distribution in Fig. 5 shows that the majority of the pore volume of activated carbon 208C (about 45%) is located in pores with a half-width (i.e., the distance from the pore center to the inner wall; for slit pores, half the slit width) of 2.5–5 Å. About 20% is located in pores with smaller half-widths, although the exact distribution is outside the measured values. About 25% of the pore volume is concentrated in pores with a half-width between 5 and 7.5 Å and 10% in pores with a half-width between 10 and 12.5 Å. For SC2, the distribution is comparable, with the same quantity of pore volume in absolute terms derived from pores with a half-width below 5 Å as for 208C. After that, SC2 has significantly less volume in the pores with a larger half-width. Overall, this results in the lower total pore volume of the activated carbon SC2 compared to 208C. Both samples hardly show any pores with a half-width between 7.5 and 10 Å and over 12.5 Å.

B. Adsorption capacity measurements with hydrogen

The second part of the experimental study involved adsorption measurements with hydrogen. While multiple H_2 isotherms

TABLE III. Additional parameters for activated carbons SC2 and 208C, determined from the 77 K nitrogen isotherm using various analytical methods.

Parameter	SC2	208C	Unit
Half-pore width $d/2$[a]	5.39	5.72	Å
Char. energy of ads. E_0[a]	249.8	235.5	meV
External surface area[b]	12.59	17.40	m²/g

[a]Determined by the DR-plot and using Eq. (7).

[b]Determined by the t-plot method.

were recorded for SC2 and 208C (cf. Fig. 6), technical issues with the measuring cell limited measurements at 20.37 and 27 K for SC2.

Each isotherm was initially analyzed separately using the Langmuir and BET theories. The corresponding parameters were obtained using the IQ3 software (BET) and manual linear fits (Langmuir), as summarized in Tables IV and V. These models yield characteristic parameters for each temperature: the monolayer volume V_{mono} and either the Langmuir constant b or the BET constant C.

However, both approaches lack consistency across temperatures, as V_{mono} exhibits a pronounced dependence on T. This provides evidence that neither the Langmuir nor the BET models are appropriate for accurately describing the adsorption behavior over
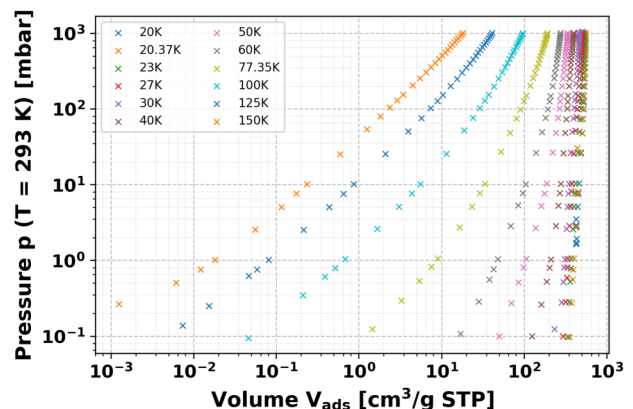

FIG. 6. Hydrogen isotherms for activated carbon 208C over a wide temperature range.

TABLE IV. Langmuir theory parameters of hydrogen adsorption on SC2 and 208C activated carbons analyzed with iQ3 software for a wide range of cryogenic temperatures (20–150 K).

Temperature	SC2		208C	
	$V_{\text{mono, STP}}$ (cm³/g)	b (mbar⁻¹)	$V_{\text{mono, STP}}$ (cm³/g)	b (mbar⁻¹)
20 K	—	—	555	1.15×10^{-1}
23 K	474	1.24×10^{-1}	538	9.10×10^{-2}
27 K	—	—	514	4.89×10^{-2}
30 K	424	7.57×10^{-2}	474	4.91×10^{-2}
40 K	375	3.60×10^{-2}	405	3.07×10^{-2}
50 K	327	2.53×10^{-2}	347	2.41×10^{-2}
60 K	280	1.74×10^{-2}	289	1.65×10^{-2}
77 K	208	6.90×10^{-3}	218	5.95×10^{-3}
100 K	126	2.91×10^{-3}	128	2.63×10^{-3}
125 K	84	9.76×10^{-4}	84	9.18×10^{-4}
150 K	76	3.26×10^{-4}	77	3.03×10^{-4}

an extended temperature range, given that V_{mono} is, by definition, expected to be independent of temperature in both theoretical models.

The Dubinin–Radushkevich (DR-)theory provides a physically grounded framework for subcritical adsorption, relying on the saturation vapor pressure p_s, which is defined only below hydrogen's critical temperature (33.15 K). All subcritical isotherms were therefore transformed into $\ln V_{\text{ads}}$ vs $(k_B T \ln (p/p_s))^2$ plots (see Fig. 7) and analyzed jointly. The data followed the DR-theory well over a broad range, with a clearly identifiable linear curve segment.

This linear region can be described consistently for all subcritical isotherms using only two temperature-independent parameters, enabling the prediction of isotherms at arbitrary subcritical temperatures. At low values of $(k_B T \ln (p/p_s))^2$, i.e., high pressures relative to p_s, corresponding to regions where more than 90% of the micropore volume is filled, systematic deviations from linearity occurred, with measured adsorption exceeding the DR-predicted micropore volume. This behavior is also evident when comparing the three theories for a single isotherm (e.g., 27 K in Fig. 8): DR accurately describes the low-pressure regime, whereas Langmuir and BET better capture the high-pressure adsorption behavior.

Micropore volumes obtained via DR were $V_p = 388 \, \text{cm}^3/\text{g}$ (STP) for SC2 and $V_p = 417 \, \text{cm}^3/\text{g}$ (STP) for 208C, while the

TABLE V. BET theory parameters of hydrogen adsorption on SC2 and 208C activated carbons analyzed with iQ3 software for subcritical temperatures (20–30 K).

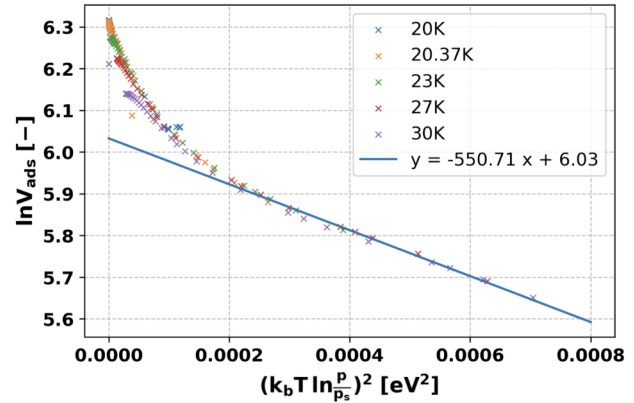| Temperature (K)	SC2		208C	
	$V_{\text{mono, STP}}$ (cm³/g)	C (—)	$V_{\text{mono, STP}}$ (cm³/g)	C (—)
20	—	—	503	2 223
23	422	2 945	487	1 724
27	—	—	470	925
30	342	21 683	383	15 042

FIG. 7. DR plot with best-fit line (activated carbon 208C).

values for the DR constants were $D = 516 \, \text{eV}^{-2}$ and $D = 551 \, \text{eV}^{-2}$, respectively.

Overall, the DR-theory offers a consistent and physically motivated description of H_2 adsorption on the activated carbons in the subcritical regime at low relative pressures with respect to p_s. Unlike Langmuir and BET, which require separate fits for each temperature, DR enables accurate prediction of adsorption under conditions matching those encountered in cryosorption pump operation (cf. Sec. V).

The Autosorb iQ3 conducted measurements automatically and did not provide experimental error bars. However, based on hardware specifications and applied corrections, the following uncertainties can be estimated: pressure readings were taken with capacitive sensors specified to 1% absolute accuracy; temperatures at the pressure sensors were monitored with an accuracy of 0.1 K, while adsorption temperatures fluctuated within 0.5 K, potentially resulting in a maximum uncertainty of approximately 2% in the
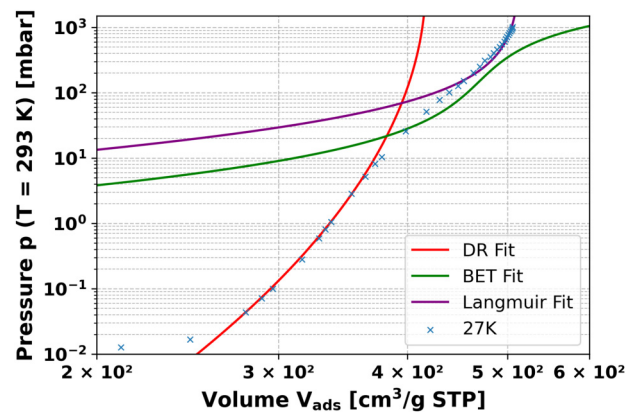

FIG. 8. Comparison of theoretical fits (DR, BET, Langmuir) to hydrogen adsorption isotherm on activated carbon 208C at 27 K.

measured adsorbed volume. Corrections for nonideal gas behavior and thermal transpiration were applied automatically. The temperature profile between the pressure sensors and the adsorption cell was manually corrected for adsorption processes during calibration measurements below 100 K, contributing an estimated additional uncertainty of 1%. All fits for nitrogen and hydrogen yielded correlation coefficients above 0.99, and parameter uncertainties for the manual DR and Langmuir fits remained below 2%. The reported parameters are therefore considered accurate within the estimated uncertainties from measurement and fitting.

C. Binding energies of H_2 on activated carbons SC2 and 208C

The Clausius–Clapeyron equation,

$$\left[\frac{d\ln p}{d\frac{1}{T}}\right]_{V_{ads}} = -\frac{E_{ads}(V_{ads})}{k_b},\qquad(9)$$

allows determination of the isosteric adsorption energy E_{ads} as a function of relative pore filling V_{ads}/V_p.[12] This requires deriving isosteres—i.e., curves of constant adsorbed amount in the pressure—temperature domain—from the measured isotherms. Isosteres are plotted as $\ln(p)$ vs $1/T$, and E_{ads} is obtained from the slope of the resulting curves.

Unlike the DR-theory, which assumes a constant adsorption energy E_0, the Clausius–Clapeyron approach yields a coverage-dependent E_{ads}, better reflecting physical conditions.

Given the good agreement of the measured H_2 isotherms with the DR theory (Fig. 6), a theoretical expression for the coverage-dependent E_{ads} can be derived analytically. To achieve this, the Clausius–Clapeyron equation, which relates the slope $d\ln(p)/d(1/T)$ to E_{ads}, is applied following a reordered form of the DR isotherm [cf. Eq. (6)], where the pressure p is expressed as a function of inverse temperature $1/T$,

$$E_{ads} = \sqrt{\frac{\ln\left(V_{ads}/V_p\right)}{-D}}.\qquad(10)$$

Figure 9 shows the isosteric adsorption energies determined from both the DR constants and the isosteres as a function of V_{ads}/V_p. The determined adsorption energies fall clearly within the range of physisorption, which implies a strictly reversible adsorption process.

For comparison, Fig. 9 also includes $E_{ads}(\Theta)$ for H_2 adsorbed on electropolished stainless steel, based on DR constant obtained by Chill et al.[5] For simplicity, this comparison assumes that the ratio of H_2 coverage on the stainless steel surface $\Theta_{ss} = \sigma/\sigma_{mono}$ can be compared to the H_2 gas loading ratio of the activated carbon, i.e., $\Theta_{carb} = V_{ads}/V_p$.

As expected, H_2 adsorption energies on activated carbon exceed those on stainless steel. It is noteworthy that the adsorption energies of the activated carbon SC2 exhibit a slight superiority over those of the 208C, despite the latter's capacity being higher at the same occupancy. A potential explanation, when considered
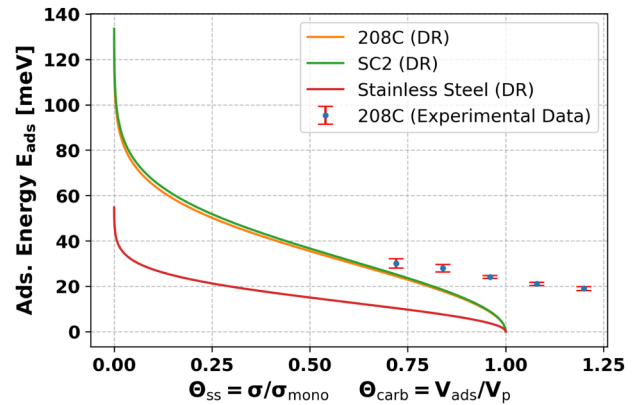

FIG. 9. Comparison of the coverage-dependent adsorption energies of H_2 on activated carbon types (SC2, 208C) and stainless steel (ss).

alongside the DFT pore size distribution, is that at SC2, a greater proportion of adsorption occurs within pores with a narrower half-width in comparison to the adsorption observed for 208C. This likely reflects stronger binding in narrower pores, which enhances total adsorption energy.

At surface coverages above 85% of the DR micropore volume, significant deviations from the DR model occur—consistent with the behavior in Fig. 7.

V. THE SIS100 CRYOSORPTION PUMPS

The results presented herein suggest that activated carbon Aquacarb 208C can be utilized as an adsorbent material for the SIS100 cryosorption pumps, given its higher adsorption capacity compared to that of SC2. The SIS100 vacuum system design calls for 83 additional cryosorption pumps along the cryogenic beam line. Due to spatial constraints within the SIS100 cryostats, only lumped cryosorption pumps can be used. The installation of 60 pumps is planned at intervals of approximately 13 m between each set of two superconductor dipoles, with the remaining 23 positioned between selected superconductor quadrupole units. The design specifications for these pumps (cf. Fig. 10) have been previously outlined elsewhere,[3] so only the main features of the pumps are summarized here.

Each pump is mounted on a conventional DN100CF flange, housed in a standard CF nipple, and consists of six circular copper panels each attached to an axially arranged LHe cooling system within the nipple using copper screws. The central cooling tube accommodates both the LHe supply and LHe return line, thereby enabling efficient and homogeneous cooling of all adsorbent cryo-panels to 4.5 K. Each panel is double-sided coated with the chosen granular adsorbent material, Aquacarb 208C, using a low-temperature-resistant epoxy resin. A fine-mesh grid prevents loose activated carbon particles from entering the beam pipe, with negligible impact on pumping speed. The averaged coating density of the panels is 0.04 g/cm², equivalent to 30 g per pump.

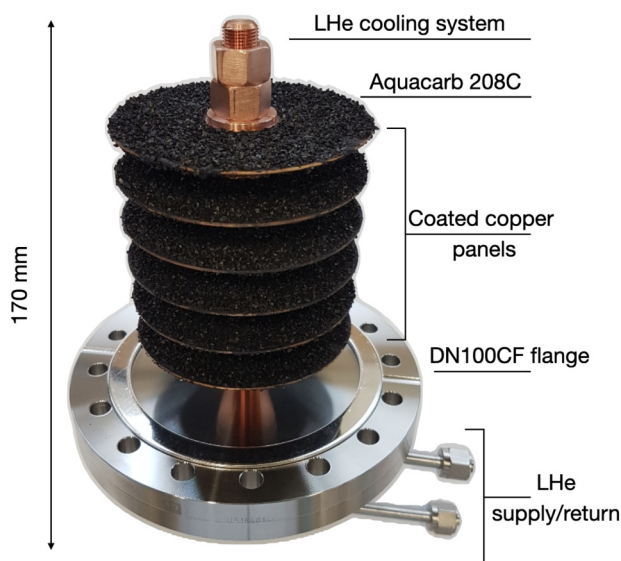**FIG. 10.** SIS 100 cryosorption pump.

Based on the adsorption measurements, each pump can adsorb a gas volume of $V_{ads} = 30 \times 417 \, cm^3/g(STP) = 12\,510 \, cm^3$ (STP), which corresponds to a maximum H_2 amount of $Q_{max,th} \approx 209 \, mbar\,l$ at a gas temperature of $T = 4.5\,K$. This prompts the critical inquiry of determining the practical maximum quantity of H_2 gas, $Q_{max,p}$, that the pump may adsorb, such that the vapor pressure of the gas phase above the adsorbent remains below the operational upper pressure limit of some $\sim 1 \times 10^{-12}$ mbar (at $4.5\,K$), as is necessary in the cryogenic accelerator sections for beam operation.
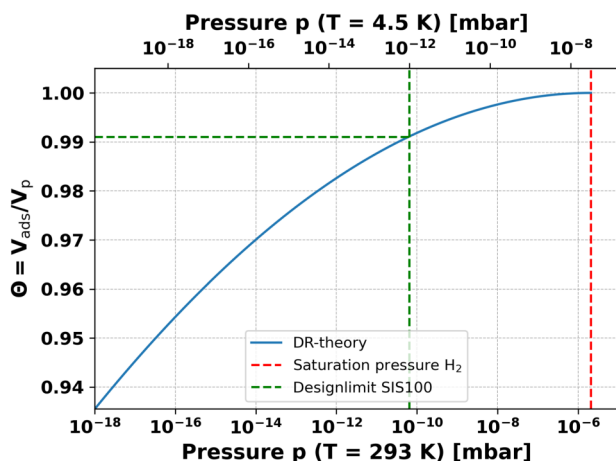

FIG. 11. Adsorption isotherm for the system H_2-activated carbon 208C calculated using the DR-theory for $T = 4.5\,K$ and p_s ($T = 293\,K$) $= 2.1 \times 10^{-6}$ mbar.

$Q_{max,p}$ can be calculated by examining the isotherm, which indicates the maximum permissible gas coverage of the adsorbent before the vapor pressure exceeds the upper pressure limit. Using the determined DR constant, the adsorption isotherm depicted in Fig. 11 is obtained for H_2—Aquacarb 208C at $4.5\,K$. As evident from the modeled isotherm, the activated carbon has the capacity to adsorb H_2 up to a point close to saturation ($\Theta = V_{ads}/V_p \approx 99\%$) before the vapor pressure exceeds the $\sim 1 \times 10^{-12}$ mbar threshold. It must also be taken into account that the epoxy resin blocks the adsorbable surface area of activated carbon by approximately 1%. Consequently, based on DR-theory, a pump with $30\,g$ of adsorbent material can practically adsorb approximately $Q_{max,p} \approx 205 \, mbar\,l$, at $4.5\,K$, while meeting the SIS100 pressure requirements.

VI. SUMMARY AND CONCLUSION

This study examined the adsorption properties of activated carbons SC2 and Aquacarb 208C. Nitrogen adsorption isotherms were measured, and the results showed that 208C exhibited greater pore volumes and adsorption capacities than SC2. Density functional theory (DFT) analysis of the pore size distribution revealed a similar pattern for both carbons. For hydrogen, 208C exhibited a higher adsorption capacity than SC2. The DR analysis proved reliable for describing hydrogen adsorption on both activated carbons across a broad subcritical temperature and pressure range. The DR analysis yielded a temperature-independent pore volume of $V_p \approx 388 \, cm^3/g$ (STP) for SC2 and $V_p \approx 417 \, cm^3/g$ (STP) for 208C.

The results support the use of 208C in SIS100 cryosorption pumps. Subsequent analysis determined that a single pump operating at $4.5\,K$ can adsorb up to $205 \, mbar\,l$ of H_2 while maintaining the SIS100 vacuum pressure below 1×10^{-12}. The DR analysis also enabled calculation of the surface coverage-dependent adsorption energies $E_{ads}(\Theta)$. H_2 adsorption energies on activated carbon were significantly higher than on electropolished stainless steel. This finding is important in the event of a sudden loss of cooling capacity in the liquid helium (LHe) supply of the accelerator, as the beam pipes would then warm up and the hydrogen previously cryosorbed on the cold surfaces could be released, causing pressure spikes. Since both the beam pipes and the cryosorption pumps in the SIS100 are connected to the same LHe cooling circuit, the chambers and pumps warm up simultaneously. However, due to the differing binding energies, hydrogen desorbs from the inner surfaces of the stainless steel pipes at lower temperatures than from the activated carbon in the cryosorption pumps. Temperature-programed desorption (TPD) theory shows that, in the event of a sudden onset of a temperature rise that proceeds linearly in time, hydrogen adsorbed on a stainless steel surface reaches its desorption maximum as early as $17\,K$. In contrast, hydrogen adsorbed on activated carbon reaches its desorption maximum only at approximately $26\,K$.

preparing and providing the scanning electron micrographs images of the activated carbon samples.

AUTHOR DECLARATIONS

Conflict of Interest

The authors have no conflicts to disclose.

Author Contributions

Nick P. Zobel: Conceptualization (equal); Data curation (equal); Formal analysis (equal); Investigation (equal); Methodology (equal); Visualization (equal); Writing – original draft (equal). **Stefan Wilfert:** Conceptualization (equal); Formal analysis (equal); Visualization (equal); Writing – original draft (equal). **Klaus Blaum:** Conceptualization (equal); Supervision (equal); Writing – review & editing (equal). **Sven M. Elbert:** Investigation (equal); Methodology (equal); Validation (equal); Writing – review & editing (equal). **Michael Mastalerz:** Resources (equal); Supervision (equal); Writing – review & editing (equal). **Peter J. Spiller:** Project administration (equal); Supervision (equal); Writing – review & editing (equal).

DATA AVAILABILITY

The data that support the findings of this study are available from the corresponding author upon reasonable request.

REFERENCES

[1] P. Spiller et al., J. Instrum. **15**, T12013 (2020).
[2] P. J. Spiller et al., "Advanced concepts and technologies for heavy ion synchrotrons," in Proceedings of IPAC'21 (JACoW Publishing, Geneva, Switzerland, 2021), pp. 594–597.
[3] S. Tippmann, T. Jande, S. Hempel, A. Kade, J. Klier, S. Wilfert, and I. Pongrac, "Adaptable cryosorption pump system for SIS100," in Proceedings of the IIR International Conference on Cryogenics 2019 (International Institute of Refrigeration, Paris, France, 2019).
[4] V. Baglin, "Cryopumping and vacuum systems," CAS—CERN Accelerator School: Vacuum for Particle Accelerators, arXiv:2006.01574 (2020).
[5] F. Chill, S. Wilfert, and L. Bozyk, J. Vac. Sci. Technol. A **37**, 031601 (2019).
[6] R. Verma, H. N. Nagendra, G. A. Vivek, S. Kasthurirengan, N. C. Shivaprakash, and U. Behera, Cryogenics **108**, 103089 (2020).
[7] C. Day, A. Antipenkov, M. Dremel, H. Haas, V. Hauer, A. Mack, D. K. Murdoch, and M. Wykes, Vacuum **81**, 738 (2007).
[8] M. Scannapiego and C. Day, IOP Conf. Ser.: Mater. Sci. Eng. **278**, 012160 (2017).
[9] V. Krishnamoorthy, S. S. Udgata, V. S. Tripathi, R. Gangradey, S. Kasthurirengan, and U. Behera, J. Phys.: Conf. Ser. **390**, 012077 (2012).
[10] J. Rouquerol, F. Rouquerol, P. Llewellyn, G. Maurin, and K. Sing, Adsorption by Powders and Porous Solids: Principles, Methodology and Applications, 2nd ed. (Academic, Oxford, 2013).
[11] M. M. Dubinin and L. V. Radushkevich, Dokl. Akad. Nauk SSSR **55**, 331 (1947) (in Russian).
[12] E. Wallén, J. Vac. Sci. Technol., A **15**, 265 (1997).
[13] M. M. Dubinin and H. F. Stoeckli, J. Colloid Interface Sci. **75**, 34 (1980).
[14] J. H. de Boer, B. C. Lippens, B. G. Linsen, J. C. P. Broekhoff, A. van den Heuvel, and T. J. Osinga, J. Colloid Interface Sci. **21**, 405 (1966).
[15] C. Lastoskie, K. E. Gubbins, and N. Quirke, J. Phys. Chem. **97**, 4786 (1993).
[16] A. V. Neimark, Y. Lin, P. I. Ravikovitch, and M. Thommes, Carbon **47**, 1617 (2009).
[17] V. Hauer and C. Day, "Cryosorbent characterization of activated charcoal in the coolsorp facility," Tech. Rep. FZKA 6745 (Forschungszentrum Karlsruhe GmbH, 2002).
[18] M. Grabellus, "Conversation with matthias grabellus, application engineer at chemviron," discussion about activated carbon 208C, personal communication (2024).
[19] I. H. Bell, J. Wronski, S. Quoilin, and V. Lemort, Ind. Eng. Chem. Res. **53**, 2498 (2014).
[20] N. P. Zobel, "On the use of gas adsorption principles to improve the vacuum in particle accelerators," B.Sc. thesis (University of Heidelberg, 2024) (in German).
[21] Autosorb iQ and ASiQwin Gas Sorption System Operating Manual (Quantachrome Instruments, Boynton Beach, FL, 2017).

22 January 2026 10:36:35